

Changes in physical architecture and lipids compounds in skeletal muscle from Pekin duck and Liancheng white duck

Hehe Tang, He Zhang, Dapeng Liu, Shunan Li, Zhen Wang, Daxun Yu, Zhan bao Guo, Shuisheng Hou, and Zhengkui Zhou ¹

Institute of Animal Science, Chinese Academy of Agricultural Sciences, Beijing 100193, PR China

ABSTRACT As a complex food, meat displays various biochemical properties that are determined to a great extent by physical architecture and lipid metabolites. Pekin duck and Liancheng white duck are elite breeds with distinct characteristics. Here, we explored the development of the muscle fibers from embryonic stage to 10-wk after birth, and muscle fibers grow slowly after 8-wk. We investigated the meat quality, ultrastructure, lipidomics profiling, and lipids spatial distribution of skeletal muscle at 8 wk. Pekin duck has lower Warner-Bratzler shear force (**WBSF**) ($P < 0.05$), high intramuscular fat (**IMF**) ($P < 0.01$), longer and wider sarcomere, and higher mitochondrial density ($P < 0.001$). Liancheng white duck with tighter collagen architecture. A total of 950 lipids from 6 lipid

classes identified with lipidomics were analyzed, the levels of GP, GL, and PR were significantly higher in Pekin duck ($P < 0.05$), SL and ST were significantly higher in Liancheng white duck ($P < 0.05$). There were 333 significantly different lipids ($|\log_2(\text{Fold Change})| \geq 1$ and $\text{FDR} < 0.05$) screened, most lipids distributed in the muscle tissue were uniform, but some specifically distributed in connective tissue. To some extent, the results demonstrate the high lipid deposition capacity of Pekin duck and the high medicinal function of Liancheng white duck. Our study provides new insights into the relationship between skeletal muscle architecture and meat toughness, which increased the knowledge of lipidomic characteristics and provide a basis for duck meat authentication.

Key words: intramuscular fat, meat quality, muscle structure, lipid profile, lipidomics

2023 Poultry Science 102:103106
<https://doi.org/10.1016/j.psj.2023.103106>

INTRODUCTION

In meat animal agriculture, the primary goal is to produce as many high-quality protein food sources as possible with the least input. There has been tremendous progress in this regard over the past several decades. In the foreseeable future, improving growth efficiency and meat quality will continue to be a significant goal of animal husbandry.

The skeletal muscle accounts for 40 to 50% of the animal's body weight (Payne and Bearden, 2006). Albrecht conclude that the muscle fiber numbers and fascicle numbers are fixed during embryonic development in cows (Albrecht et al., 2006), while the increase in muscle mass was attributed to postnatal hypertrophy of skeletal muscle fibers (Schiaffino et al., 2013). Heterogeneous muscle cells determine the muscle's overall biochemical and

contractile properties, as well as its texture and tenderness (Blackburn et al., 2019). Meat tenderness is closely related to the structural and biochemical properties of skeletal muscle fibers, especially myofibril and muscle fibers, as well as intramuscular connective tissue, endomysium, and perimysium, which are composed of collagen fibrils (Maltin et al., 2003; Matarneh et al., 2021).

Meat has played a crucial role in human evolution due to its highly abundant nutrients (Pereira and Vicente, 2013). As a complex food, the biochemical properties of meat are largely determined by a number of metabolites (Ramanathan et al., 2020). As flavor precursor volatiles, lipids metabolites in skeletal muscle provide essential nutrition (Breslin 2013; Li et al., 2021b). Metabolome analyses have been widely applied to meat phenotype studies in recent years (Jia et al., 2021; Wang et al., 2021). However, the meat metabolome has not been systematically studied, which hinders further research and improvement of meat nutrition and flavor (Muroya et al., 2020).

Skeletal muscle microstructure and localization have been studied using electron microscope, optical microscope, histochemical, and fluorescence assays (Roy et al., 2018; Huo et al., 2021). These methods, however,

© 2023 The Authors. Published by Elsevier Inc. on behalf of Poultry Science Association Inc. This is an open access article under the CC BY-NC-ND license (<http://creativecommons.org/licenses/by-nc-nd/4.0/>).

Received July 4, 2023.

Accepted September 7, 2023.

¹Corresponding author: zhouzhengkui@caas.cn

were unable to provide accurate information about the spatial distribution of each molecule. In recent years, mass spectrometry imaging (MSI) has received increasing attention due to its ability to capture the spatial distribution of metabolites at the molecular level. It has been successfully visualized by using matrix-assisted laser desorption/ionization (MALDI) (Norris and Caprioli, 2013). It has been widely used to reveal the tissue distribution characteristics of metabolites in food and plant fields (Li et al., 2018, 2020b). However, the spatial distribution of metabolites in duck meat has not been reported.

Duck is an important economic poultry, which derived from the mallard in 500 BC in central China, the meat is popular in the meat industry (Hitosugi et al., 2007). Pekin duck is a world-famous dish that is roasted (Zhou et al., 2018). Liancheng white duck is an elite indigenous breed, deeply loved by consumers due to its highly delicious flavor (Huo et al., 2021). Our study identified differences between different duck breeds in terms of physical architecture and chemical properties of skeletal muscle, which provided new insights into the skeletal muscle. Moreover, this study also contributes to the understanding of muscle development and improves meat production and quality in livestock.

MATERIALS AND METHODS

Ethics Statements

Chinese National Research Council regulations were followed and the Science Research Department of the Institute of Animal Sciences, Chinese Academy of Agricultural Sciences, China (IAS2022-103) approved the animal experiments. Experimental procedures and methods were conducted in accordance with approved guidelines to ensure animal welfare.

Sampling

Ducks were injected with duck viral hepatitis vaccine at 1-day old after hatching, and injected with avian

influenza virus vaccine at 15-days old after hatching. Individuals with similar body weight and well health were selected for breast muscle collection. Breast muscles were collected from the right sides of Pekin duck and Liancheng white duck in different growth stages, as well as 9 growth stages from the 14-d and 21-d (embryonic stage), 1-d, 1-wk, 3-wk, 5-wk, 6-wk, 8-wk, and 10-wk after hatching, and the gender consistency (♀). In this study, 14 samples were selected at each stage used to hematoxylin and eosin staining (H&E). Cut from designated blocks of each breast muscle to determine muscle fiber phenotype (Figure 1, blocks A).

Hematoxylin and Eosin Staining

The breast muscles were decalcified, dehydrated, embedded in paraffin blocks, and sectioned after being preserved in 4% paraformaldehyde. Specimens were stained using H&E and examined by light microscopy, total 3 visual fields were selected for each section to take pictures. A total of 6 muscular histological traits were collected, which include muscle bundle diameter, muscle bundle area, fiber diameter, fiber area, fiber density, and perimysial thickness (Figure 1B and C). Image-Pro Plus 6.0 software (Media Cybernetics, Silver Spring, MD) was used to calculate the histological traits at least 30 fragments in each sample for histological feature calculation.

Meat Quality Traits Analysis

Cut from designated of each breast muscle used for meat quality traits analysis (Figure 1A, number 1, 2, 3). Meat color was evaluated according to the CIE scale: lightness (L^*), redness (a^*), and yellowness (b^*). Using Minolta CR-400 Chroma meter (8 mm aperture, 2° viewing angle, D65 illuminant, Konica Minolta Sensing Inc., Osaka, Japan) to measure the CLE L^* , a^* , b^* light reflectance, and calibrate using a standard whiteboard ($Y = 84.4$, $x = 0.3195$, $y = 0.3368$). After 45 min of exposure to air, determine the color parameters of the meat

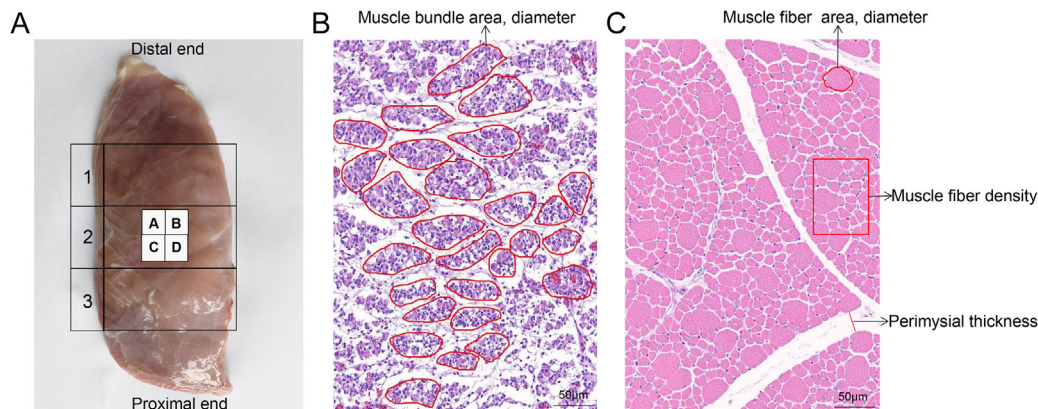


Figure 1. The sampling from the breast muscle of duck and phenotype collection. (A) Sample of 1, 2, 3 used for meat quality traits analysis. Blocks A used for H&E, and blocks B used for sarcomere, mitochondria, and collagen architecture observation by TEM and SEM. Blocks C and D used for lipid profiling and MALDI. (B, C) Myofiber phenotype collection, including muscle bundle diameter, muscle bundle area, fiber diameter, fiber area, fiber density, and perimysial thickness.

at 3 different locations on the freshly cut surface. The pH was measured at 24 h using a portable pH meter (HI99163, HANNA Instruments Inc., RI, Italy) at 3 different locations of breast muscle, calibrated with standard buffers (pH 4.0 and pH 7.0). Warner-Bratzler shear force (**WBSF**) value at 24 h postmortem was determined as previously described (Yuan et al., 2012). Breast muscles samples (2 cm × 2 cm × 2 cm) were placed in ziplock plastic bags, samples were bathed in 80°C water to a core temperature of the sample reaches 70°C, cooled to room temperature for 30 min and stored at 4°C overnight. Cut cooked samples into 3 strips (1 cm × 1 cm × 2 cm) for WBSF measurement, and 4 strips (1 cm × 1 cm × 1 cm) parallel to muscle-fiber direction for texture profile analysis (**TPA**). TPA and WBSF were estimated by texture analyzer (Stable Micro Systems Ltd., UK). The TPA textural parameters are as follows: trigger force and crosshead speed (5.0 g, 1 mm/s); working distance (5% strain), time interval (5.0 s) between the first and the second compressions.

Determination of Intramuscular Fat Content

Using anhydrous ether as the solvent, the content of IMF was determined using soxhlet extraction method. Samples were processed by a vacuum freeze-dryer to obtain meat powder for subsequent testing. The IMF content was quantified as a percentage of muscle tissue by weight. IMF was determined as previously described (Tang et al., 2023).

Transmission Electron Microscopy

The skeletal muscle cut from Figure 1A (blocks B) used for observing organelles by transmission electron microscopy (**TEM**). TEM was used to check the microstructure of breast muscle. Briefly, the skeletal muscle samples were fixed in 2.0% glutaraldehyde at 4°C. Approximately 1 mm³ small cubes from the fixed muscle samples were excised and postfixed in osmium tetroxide (1.5%) for 1 h at room temperature. These samples were dehydrated with a graded series of ethanol (30, 50, 70, 90, 95, and 100%) and embedded in epoxy resin. Ultrathin (50–70 nm) longitudinal sections (parallel to the myofibers direction) were stained with uranyl acetate and lead citrate and examined under a TEM (HITACHI, HT7700, Japan).

Scanning Electron Microscopy

The skeletal muscle cut from Figure 1A (blocks B) was used for observing perimysium collagen architecture by scanning electron microscopy (**SEM**). The samples were fixed in glutaraldehyde (2.0%) at 4°C. The perimysium collagen architecture of skeletal muscle was observed by Ohtani method (Ohtani et al., 1988), and Roy et al. (Roy et al., 2018). Briefly, the fixed sample block was cut into small pieces measuring 1 to 1.5 mm thickness (transverse with muscle fibers direction),

washed with PBS, and put into in 0.2 M phosphate buffer saline solution by immersion for 1 h. Then immerse in a 2 N (8%) NaOH solution at room temperature (25°C) for 5 to 7 d with at least 2 to 3 changes of fresh NaOH. The tissue will be like jelly and handle properly. The muscle samples were then placed into aqueous tannic acid (1%) for 4 h, rinsed with DI water with at least 3 changes, and fixed in aqueous osmium tetroxide (1.5%) for 2 h. Then, dehydrated the muscle samples by graded ethanol (30, 50, 70, 90, 95, and 100%). Remove ethanol and add t-butyl alcohol [(CH₃)₃COH, FW: 74.12] at least 3 changes, then keep the vials with sample in refrigerator to freeze for 15 to 20 min and do freeze drying. Finally, samples are ready for SEM (HITACHI, SU3500, Japan).

Lipid Profiling of Skeletal Muscle

The skeletal muscle cut from Figure 1A (blocks C) was used for lipid profiling. The samples were thawed at 4°C, weighed 20 ± 1 mg and added to a numbered homogenized centrifuge tube. One milliliter of lipid extract (methyl tert-butyl ether: methanol = 3:1) was added and homogenized with steel balls to extract lipids. Swirl the mixture for 5 min after removing the steel balls. Then, add 200 μL water, and the mixture was swirled for 5 min, centrifuged at 12,000 rpm at 4°C for 10 min. After, 300 μL of supernatant was pipetted and concentrated. We dissolved the dried supernatant in 200 μL of mobile phase B (acetonitrile/isopropanol, 10/90, 0.1% acetic acid, and 10 mmol/L ammonium formate) for liquid chromatography-tandem mass spectrometry (**LC-MS/MS**) analysis. The LC analysis conditions were as follows: column is Thermo Accucore C30 (2.6 μm, 2.1 mm × 100 mm), flow rate is 0.35 mL/min, temperature is 45°C and injection volume is 2 μL; mobile phase includes A: acetonitrile/water (60/40, V/V), B: acetonitrile/isopropanol (10/90, V/V); gradient program (20% B/0 min, 30% B/2.0 min, 60% B/4 min, 85% B/9 min, 90% B/14 min, 95% B/15.5 min, 95% B/17.3 min, 20% B/17.5 min, 20% B/20 min). Analysis using LC-ESI-MS/MS system (QTRAP), and equipped with an ESI Turbo Ionspray interface controlled by Analyst 1.6.3 software (ABSciex). The ESI source operation parameters were as follows: electrospray ion source temperature is 500°C; ion source gas I (**GSI**), gas II (**GSI**), and curtain gas (**CUR**) were 45 psi, 55 psi, and 35 psi, respectively; ion spray voltage (**IS**) (+) 5,500 V and (–) 4,500 V; collision gas (**CAD**) was medium. Each ion pair is scanned and detected according to the declustering potential (**DP**) and collision energy (**CE**).

MALDI Imaging Sample Preparation

The sample cut from Figure 1A (blocks D), freezing breast muscle of ducks were embedded in 10% gelatin (wt/vol) solutions. Briefly, breast muscle were kept in silastic mold (2 cm × 2 cm × 2 cm), then transferred to –80°C freezer, after 30 min, the sections of 10 μm

thickness were performed at -20°C using a freezing microtome equipped (Leica Biosystems, Germany). The imaging mass spectrometer (iMScope TRIO, Shimadzu, Shimadzu, Japan) was used in negative and positive ion mode for data acquisition, and using IMAGEREVEAL version 1.01 and Imaging MS Solution version 1.30 software to analysis. In this study, the mass range of ion distribution in positive and negative ion detection modes is m/z 400–900 (resolution set to $50\ \mu\text{m} \times 50\ \mu\text{m}$, $10\ \mu\text{m} \times 10\ \mu\text{m}$). Laser irradiation was applied to the tissue surface, laser irradiation diameter was set 2 (approximately $25\ \mu\text{m}$). The constant voltages of the microchannel plate detector and the sample stage were 3.50 Kv/positive, 3.0 Kv/negative, and 1.75 Kv, and the laser intensity was maintained at 60. The laser is calibrated with ink, before conducting experiments using MSI instruments, initial calibration of the precise mass was performed using the DHB matrix.

Quantitative PCR Analysis of Collagen Marker Genes

To study the expression of collagen marker genes (*COL1A1*, *COL2A1*, *COL3A1*) and muscle fiber type marker genes (*MYH7B*, *MYH1A*, *MYH1B*) in Pekin duck and Liancheng white duck, extracting the total RNA from the breast muscle. The RNA concentration and integrity were estimated using NanoDrop spectrophotometer (Thermo Fisher Scientific), and using the agarose gel method to verify. The qualified samples were used for further analysis. The cDNA synthesis was performed using a HiScript III All-in-one RT SuperMix Perfect (Vazyme) for qPCR. Then, qPCR was performed on QuantStudio 5 (Applied Biosystems, US), the qPCR conditions were as follows: initial denaturation (95°C for 30 s); followed by 40 cycles (95°C for 8 s, 60°C for 20 s), melting curve (95°C for 15 s, 60°C for 1 min, 95°C for 15 s). The relative quantifications of marker genes were analyzed by the $2^{-\Delta\Delta\text{Ct}}$. And primers were listed in Table 1, *GAPDH* was used as the reference gene.

Statistical Analysis

Data are presented as mean \pm standard error of the mean (SEM). The Student *t* test was performed by

SPSS 24.0 software (SPSS standard version 24.0, SPSS Inc., Chicago, IL). $P < 0.05$ indicated a significant difference. Principal component analysis (PCA) and partial least squares discriminant analysis (PLS-DA) using Metaboanalyst 4.0. The filtering criteria for statistical significance were variable importance in $|\log_2(\text{Fold Change})| \geq 1$, FDR < 0.05 and $P < 0.05$.

RESULTS

The Development of Skeletal Muscle

Breast muscles were collected from Pekin duck and Liancheng white duck in different growth stages (embryonic stage of 14-d to 10-wk after hatching) used for H&E. The analysis results have shown that from embryonic stage of 14-d to 1-wk after hatching, the growth rate of muscle bundle area and muscle bundle diameter was relatively slow (Figure 2A and B). The growth rate of muscle bundle area and diameter, muscle fiber area and diameter were faster from 3 wk to 8 wk, and slower after 8 wk (Figure 2A–D). In addition, the above 4 phenotypic values (muscle bundle area and diameter, muscle fiber area and diameter) of Pekin duck were significantly higher. There was a negative correlation between muscle fiber density and the above 4 phenotypes (Figure 1E). The perimysial thickness of Liancheng white duck was higher than that of Pekin duck at the early growth stage, but it was opposite at the late growth stage (Figure 1F). Therefore, the above results indicate that the breast muscle grows faster from 3 wk to 8 wk, and relatively slow growth after 8 wk.

Meat Quality Traits and IMF Content

Meat quality traits and IMF content for Pekin duck and Liancheng white duck were listed in Table 2. The WBSF of Liancheng white duck was higher than that of Pekin duck ($P < 0.05$). The hardness was significantly higher in Liancheng white duck than in Pekin duck ($P < 0.05$). The IMF content in Pekin duck was significantly higher than that in Liancheng white duck ($P < 0.001$).

Table 1. Primers for qRT-PCR of MyHC-related genes and collagen-related genes.

Gene name	Primer sequence (5' → 3')	Product size (bp)	Annealing temperature ($^{\circ}\text{C}$)	Accession number
<i>COL1A1</i>	F:GATGGGCTCACGTACAACGA R:CGCTTTCTGGGTAGACTGGG	196	60	XM_038168724.1
<i>COL2A1</i>	F:CGGCCCTAATGGTAACCCAG R:AGTCTCACCTTTGTCAACCGC	640	60	XM_038172253.1
<i>COL3A1</i>	F:CTACGATGTGAAGGCTGGCT R:CACGGTCTCCATTTCTGCCT	260	60	XM_027462007.2
<i>MYH7B</i>	F:GCTGCGGTGTAACGGTGTGTC R:CTGGAATGGCTGCTGGGT	119	60	NM_204587.2
<i>MYH1A</i>	F:GAACCCTCCCAAGTATGA R:GAGACCCGAGTAGGTGTAG	124	60	NM_001013396.1
<i>MYH1B</i>	F:GAACCCTCCCAAGTATGA R:GAGACCCGAGTAGGTGTAG	140	60	NM_204228.3
<i>GAPDH</i>	F:GGTAGTGAAGGCTGCTGCTGATG R:CGGTTGCTGTATCCATACTCGTTG	189	60	XM_038180584.1

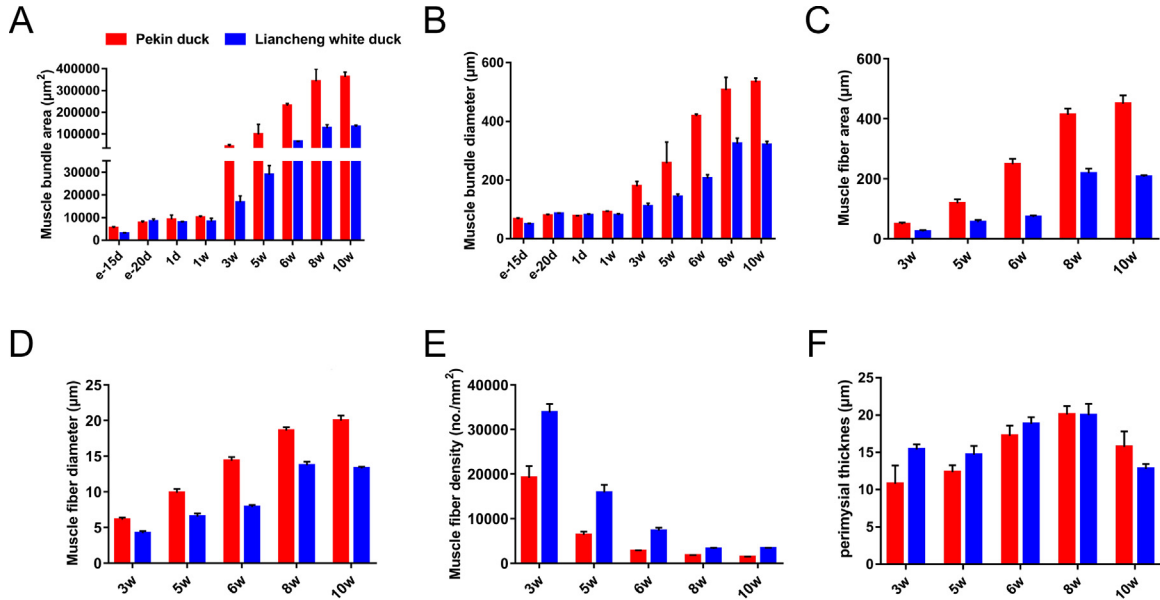


Figure 2. Myofiber development process. (A–F) The results of muscle bundle area, muscle bundle diameter, fiber area, fiber diameter, fiber density, and perimysial thickness at different growth stages, respectively.

Skeletal Muscle Under Transmission Electron Microscopy

The organelle architecture of muscle fiber is closely related to the physiological function and meat quality of skeletal muscle. To further investigate the differences in the microstructure of breast muscle between Liancheng white duck and Pekin duck, TEM was performed in this study (Figure 3A–D). Through TEM, we can clearly see the sarcomere, Z-line, M-line (Figure 3A) and mitochondria (Figure 3C). Statistical analysis of the length and width of sarcomere showed that Pekin duck was significantly greater than Liancheng white duck (Figure 3E, $P < 0.001$), the mitochondria in Pekin duck muscle fiber cells also significantly more than Liancheng white duck (Figure 3F, $P < 0.001$).

Skeletal Muscle Under Scanning Electron Microscope

The difference in skeletal muscle physical architecture is an important factor affecting meat quality, such as

Table 2. Meat quality attributes of Pekin duck and Liancheng white duck.

Items	PK	LC	<i>P</i> value
pH24h	5.82 ± 0.08	5.84 ± 0.03	0.527
L*	34.01 ± 3.85	40.24 ± 3.02	0.053
a*	17.44 ± 2.72	16.04 ± 1.98	0.127
b*	4.69 ± 0.76	5.43 ± 0.14	0.056
Warner-Bratzler shear force (N)	2625.62 ± 499.80	3220.39 ± 417.95	0.036
Texture profile analysis			
Hardness (g)	423.34 ± 173.61	743.60 ± 232.95	0.038
Springiness (ratio)	0.58 ± 0.06	0.64 ± 0.05	0.957
Cohesiveness (ratio)	0.56 ± 0.01	0.59 ± 0.02	0.052
Gumminess (g)	252.57 ± 75.51	434.14 ± 108.23	0.116
Chewiness (g)	163.35 ± 61.24	281.96 ± 82.95	0.172
Intramuscular fat content (%)	3.41 ± 0.26	2.37 ± 0.34	<0.001

the perimysium and endomysium are the main intramuscular connective tissues (IMCT) for the toughness of meat. Under SEM, it can be observed that the muscle fibers of Liancheng white duck were more closely arranged, and the muscle fibers and myogenic fibers were smaller than Peking duck (Figure S1a–f), which was also consistent with the results of H&E. In order observation perimysium collagen architecture of skeletal muscle by SEM, we explored the digestion time of samples in NaOH, the muscle architecture at different digestion time was shown in Figure S2. On the seventh day, the tissue was like jelly and handle properly, and the architecture of collagen was cleanly. The perimysium collagen architecture of the breast muscle of Liancheng white duck and Pekin duck was shown in Figure 4A, B, D, and E, the collagen architecture of Liancheng white duck were arranged thicker and tighter. Furthermore, we investigated the expression of myosin heavy chain-related genes (*MYH7B*, *MYH1A*, and *MYH1B*) and collagen-related genes (*COL1A1*, *COL2A1*, and *COL3A1*), the results showed that the expression of *MYH1A*, *COL1A1*, and *COL3A1* in breast muscle of Liancheng white duck were significantly higher than Pekin duck (Figure 4C and F).

Lipidomics Profiling

To explore the differences of lipid profiles between Pekin duck and Liancheng white duck in more detail, lipid profiles were analyzed using LC-MS/MS. We detected 950 lipids were annotated and contained 6 categories, which included glycerophospholipid (GP), glycerolipid (GL), sphingolipid (SL), fatty acyl (FA), sterol lipid (ST), and prenol lipid (PR) (Figure 5A, Table S1). The PCA and PLS-DA plots showed that a clear distinction between the 2 batches of samples, indicating that good reliability of the analytical method

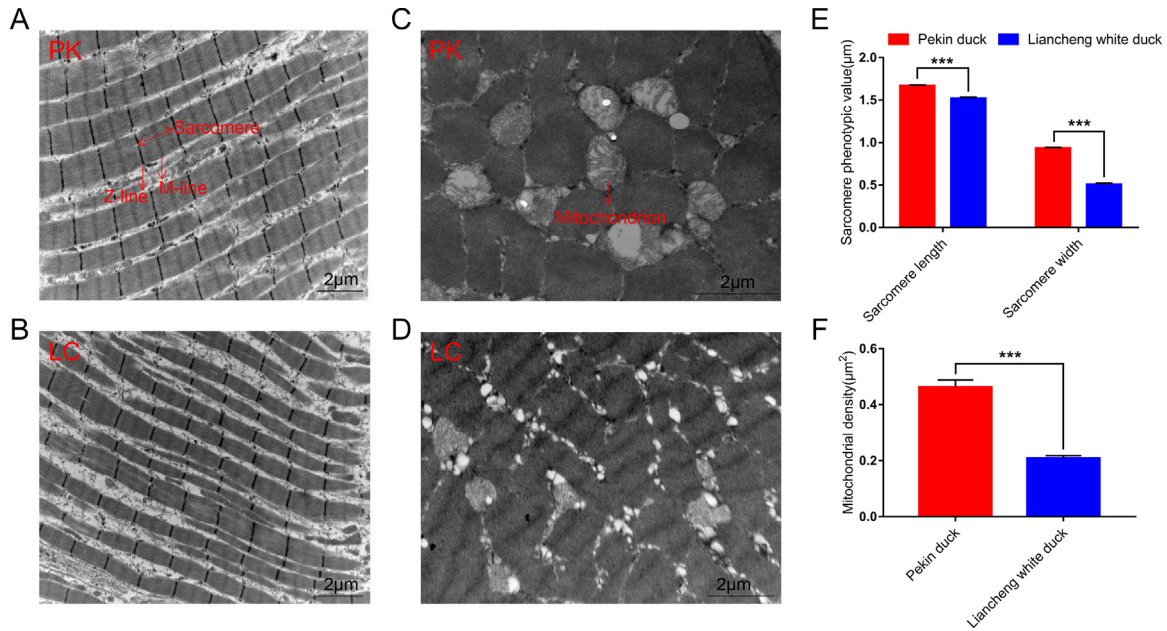


Figure 3. Myofibers under TEM. Longitudinal (A) and transverse sections (C) of Pekin duck breast muscle samples under TEM. Longitudinal (B) and transverse sections (D) of Liancheng duck breast muscle samples under TEM. Statistical analysis of sarcomere phenotype (E) and mitochondrial density (F) in Pekin duck and Liancheng white duck.

(Figure 5B and C). The correlation plot of lipids indicates a high correlation between similar lipids (Figure 5D). A heatmap analysis of lipids was conducted between Pekin duck and Liancheng white duck (Figure 5E), and the changes in the relative levels of lipids can be visually seen.

By analyzing and comparing the lipids in both breeds, it was found that the levels of GP, GL, and PR were significantly higher in Pekin duck than in Liancheng white duck, but the levels of SL and ST were significantly higher

in Liancheng white duck (Figure 5F). $|\log_2(\text{Fold Change})| \geq 1$ and $\text{FDR} < 0.05$ as criteria, a total of 333 differential lipids were identified, and 269 were significantly upregulated and 64 were significantly downregulated in Pekin duck (Figure 5G, Table S2). Comprehensive 3 index $|\log_2(\text{Fold Change})| \geq 1$, $\text{FDR} < 0.05$ and $\text{VIP} > 1$, differences lipids included 113 GPs, 80 GLs, 15 SLs, 9 FAs, 1 PR, and 1 ST (Figure 5H and I, Table S2). The lipid molecules with the highest change were summarized in Figure 6A to G.

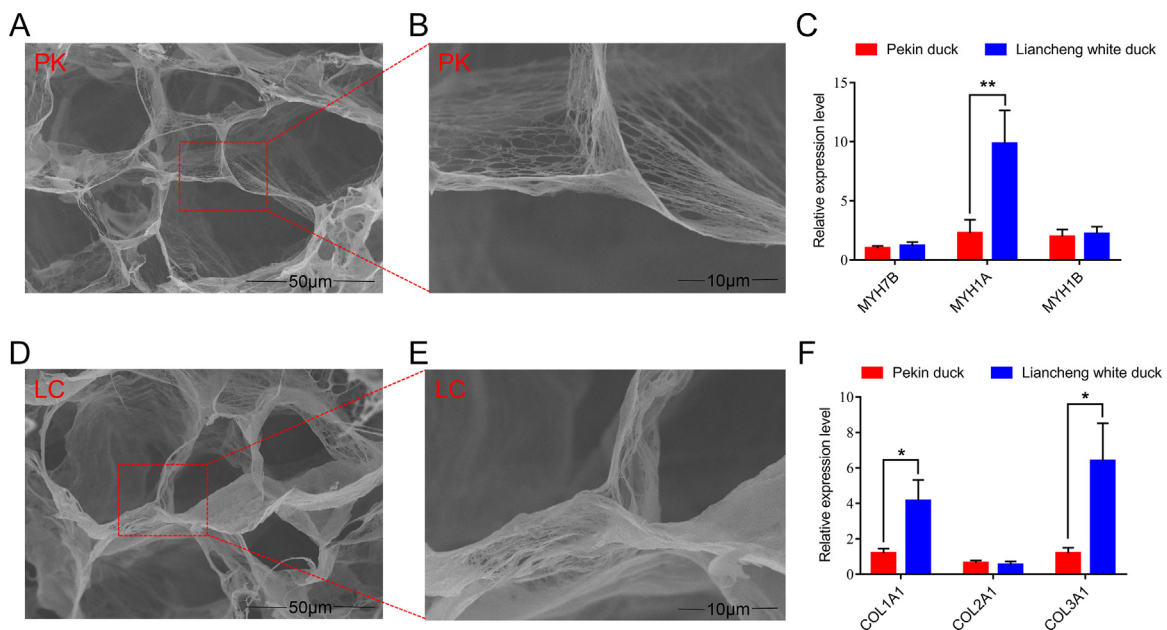


Figure 4. SEM of perimysium collagen architecture. SEM images show Pekin duck (A, B) and Liancheng white duck (D, E) perimysium collagen architecture. (C) The expression of myosin heavy chain-related genes (*MYH7B*, *MYH1A*, and *MYH1B*) by qPCR in the breast muscle of Pekin duck and Liancheng white duck. (F) The expression of collagen-related genes (*COL1A1*, *COL2A1*, and *COL3A1*) by qPCR in the breast muscle of Pekin duck and Liancheng white duck.

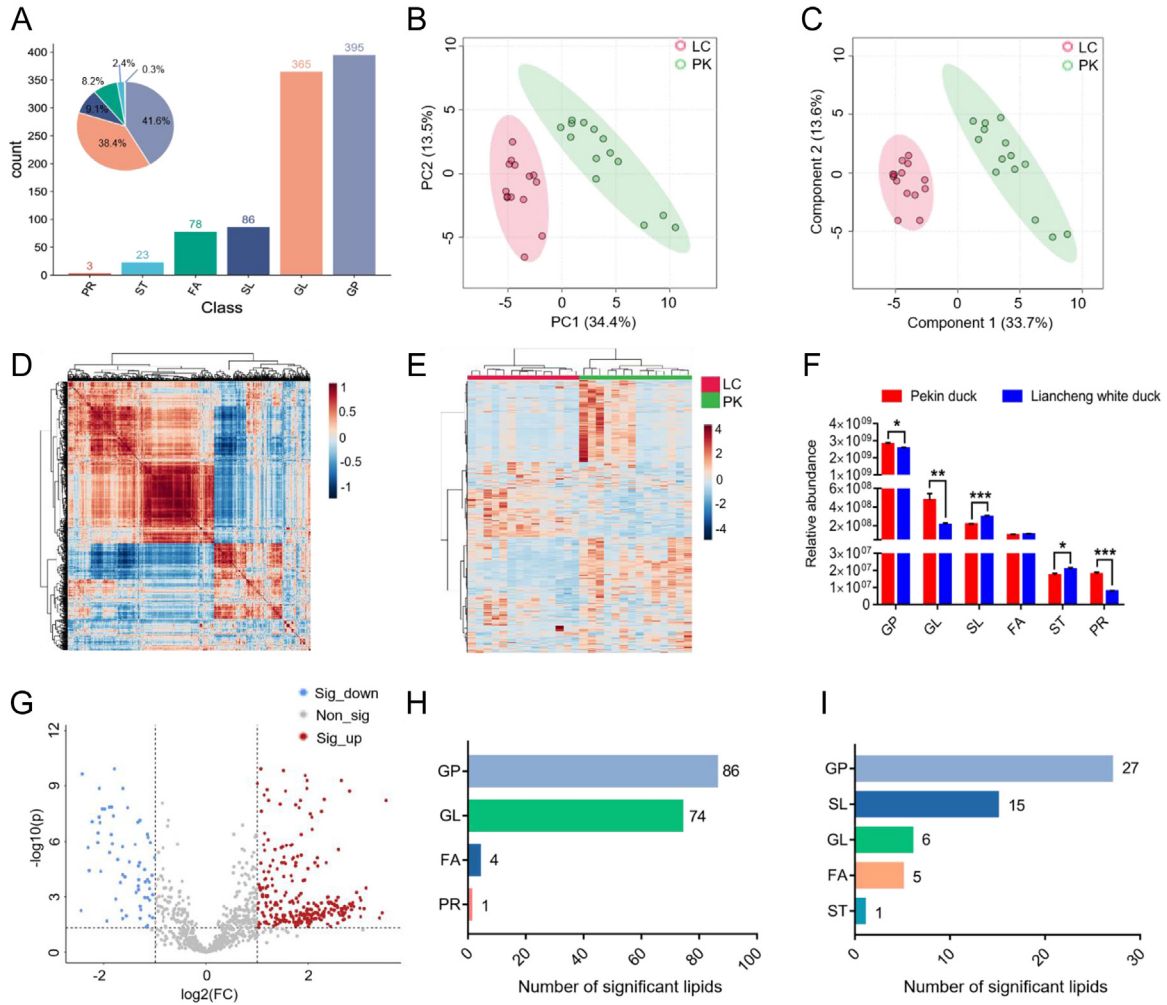


Figure 5. Lipidomic analysis revealed that the lipid profiles greatly differed between Pekin duck and Liancheng white duck. (A) A total of 950 lipids from 6 lipid classes identified with lipidomics. (B) Principal component analysis score plots. (C) Partial least squares discriminant analysis score plots. (D) Heat map of the correlation between lipids. (E) Cluster heat map of Pekin duck and Liancheng white duck breast muscle lipidome. (F) Comparison of lipid classes between Pekin duck and Liancheng white duck. (G) Volcano map of the different lipids of Pekin duck and Liancheng white duck. The number of increased (H) and decreased (I) lipid molecules in the Pekin duck. (The lipid molecules with $|\log_2(\text{Fold Change})| \geq 1$, $\text{FDR} < 0.05$ and $\text{VIP} > 1$.) * $P < 0.05$; ** $P < 0.01$, *** $P < 0.001$.

Spatial Distribution of Lipids

Visualizing the spatial distribution of lipids in skeletal muscle by MALDI mass spectrometry imaging. Figure 7A showed the schematic of muscle section of Pekin duck and Liancheng white duck. We have shown the spatial distribution of several representative differential lipids (Figure 7B–F), the mass spectra were shown in Figure 7G–I, and it can be visually seen that these lipids distributed in the muscle tissue. In addition, the lipids in the figure were all significantly different in the above lipidomics. MALDI could obtain accurate information on the spatial distribution of all detected individual molecules in the sample, but no specific spatial distribution of lipids was found, they were uniformly distributed. Therefore, we increase the spatial resolution to $10 \mu\text{m} \times 10 \mu\text{m}$, the results were shown in Figure 8, we found some lipids were specifically distributed in connective tissue, SM (d18:1_19:1), PS (17:0_22:5), and PE (20:2_18:0) were shown as representative lipid molecules.

DISCUSSION

Meat played a crucial role in human life and with highly abundant nutrients (Pereira and Vicente, 2013). Myofibers and IMCT are the 2 main structural components that contribute to the toughness of skeletal muscle, and study reported that meat with short sarcomeres is tougher than that with long sarcomeres (Wheeler et al., 2000; Maltin et al., 2003). In addition, intramuscular adipocytes closely related to meat tenderness as well (Nishimura, 2015). In this study, the determination of meat phenotype revealed that the intramuscular fat content of Pekin duck was significantly higher than Liancheng white duck ($P < 0.01$), and the WBSF was significantly lower ($P < 0.05$). By observing and analyzing the microstructure of skeletal muscle, it was found that the sarcomere length, width, and mitochondrial density of Pekin duck were significantly greater than Liancheng white duck ($P < 0.05$). The dynamic interaction between lipids and mitochondria controls the mobilization of long-chain fatty acids from lipids for

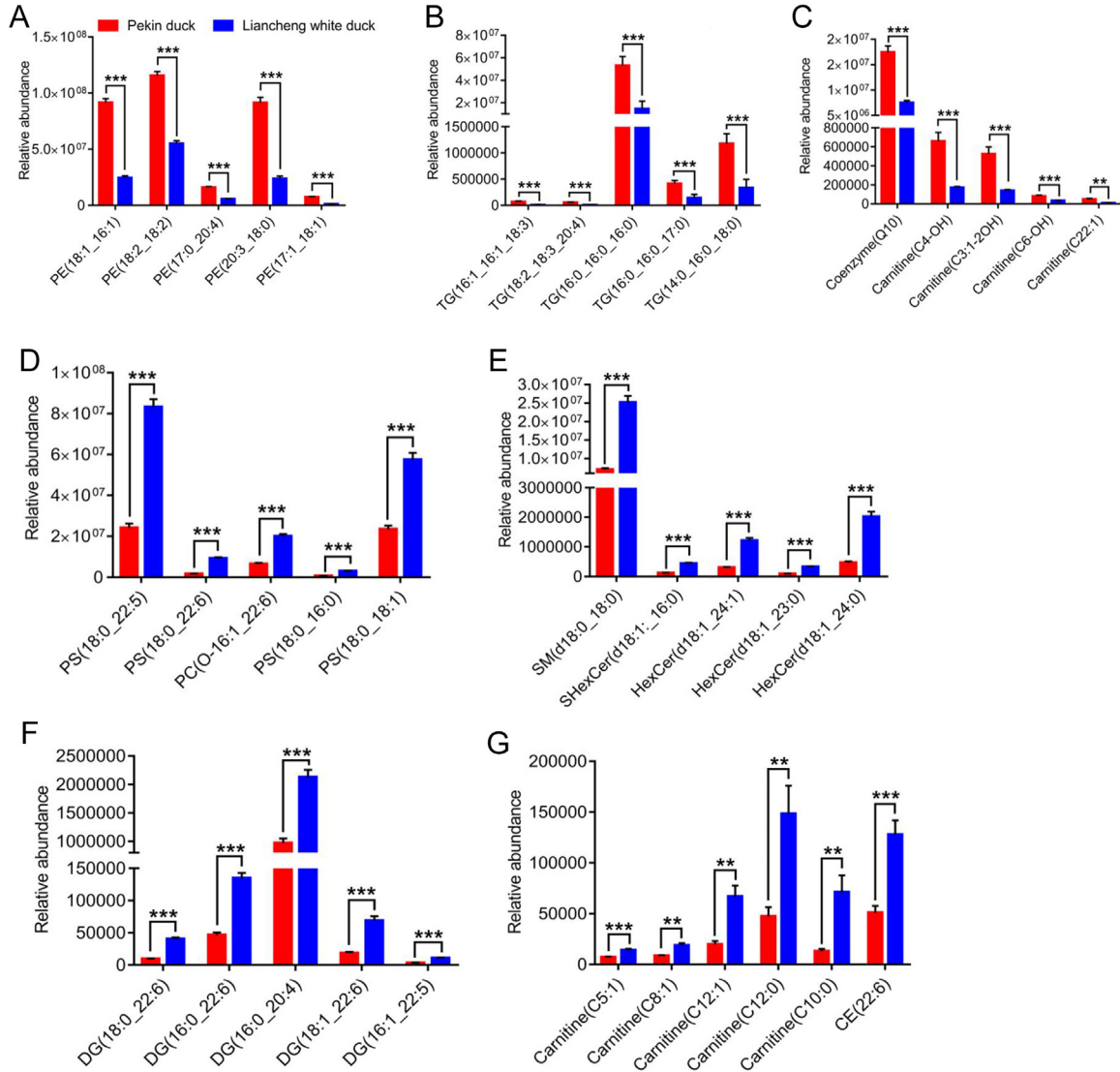


Figure 6. Significantly different representative lipid molecules. (A–C) Representative lipid molecules significantly upregulated in Pekin duck. (D–G) Representative lipid molecules significantly downregulated in Pekin duck. ** $P < 0.01$, *** $P < 0.001$.

mitochondrial β -oxidation in skeletal muscle in response to energy stress (Rambold et al., 2015; Ouyang et al., 2023). Because the growth rate and weight of Pekin duck are significantly faster and larger than Liancheng white duck, which requires more energy supply during their growth and development, and therefore, the intramuscular fat content and mitochondrial density in skeletal muscle are greater.

As the constituent unit of muscle, the effects of muscle fibers on meat quality are self-evident. By observing the skeletal muscle in 3-dimensional morphology through SEM, we can see the morphological characteristics and differences of the muscle tissue more visually. IMCT forms a series of continuous networks that integrate muscle fibers and fascia into a whole organ (Purslow, 2014). Much literature has been reported about the architecture, composition, development, and functional properties of IMCT (Kragstrup et al., 2011; Purslow, 2014). IMCT generally consists of fibrous network of collagen, which is considered to be the main contributor to the strength and stiffness of the tissue, studies found

difference in collagen fiber architecture between different myofiber types (Wojtyasiak, 2013). Accordingly, the contribution of IMCT to meat toughness is often referred to as the collagenous component. SEM observed the collagen architecture of breast muscle and found that Liancheng white duck was tighter and thicker. Study found that intramuscular fat may dilute collagen fibers and decrease shear resistance (Moloney et al., 2001), which contribute to meat tenderness (Sasaki et al., 2012). This is consistent with our study that the intramuscular fat content of Pekin duck was significantly higher than Liancheng white duck, while the WBSF was significantly lower. Study in pork has found that type II myofibers could affect the WBSF of the longissimus muscle (Orzechowska et al., 2008). Our results showed that the expression of *MYH1A*, *COL1A1*, and *COL3A1* in Liancheng white duck were significantly higher in the breast muscle of Pekin duck. Collagen, which mainly exists in muscle, bone, skin, and other tissues, widely used in biomedical, cosmetic, skincare, and other fields (Albu et al., 2014; Fan et al., 2014). Our study also explained the

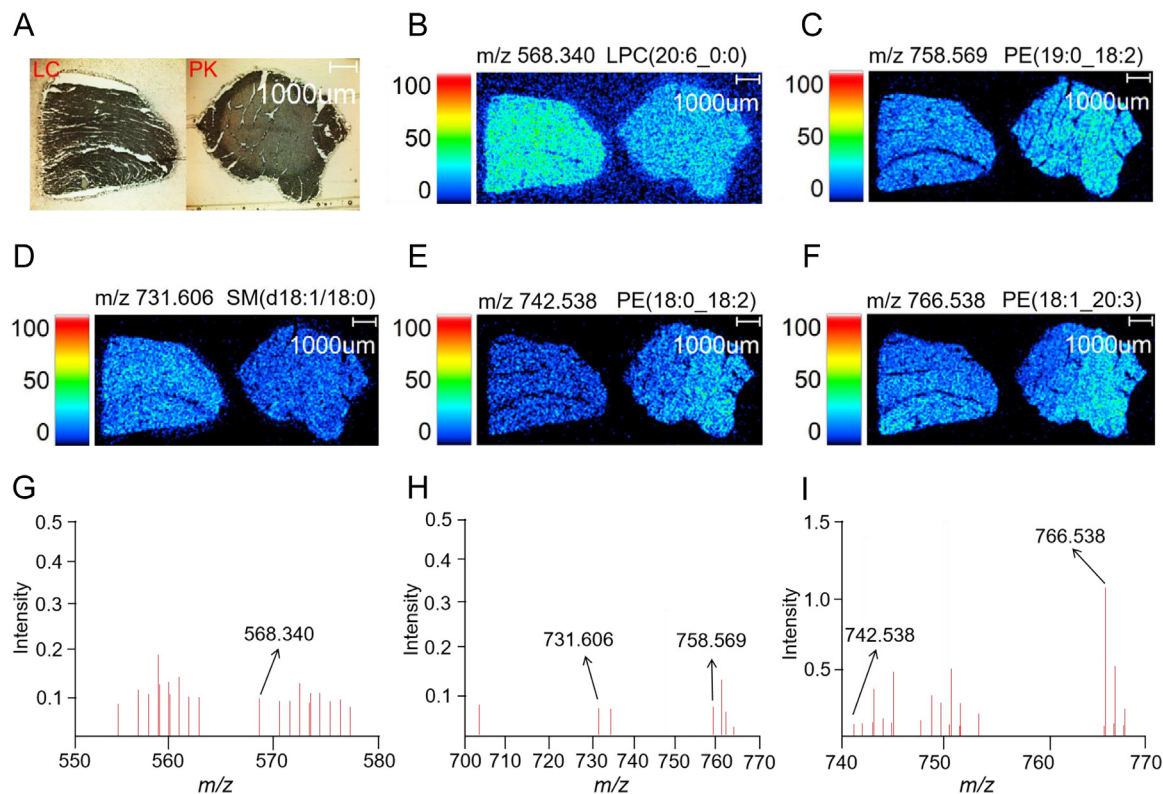


Figure 7. Spatial distribution of lipids. (A) The schematic of muscle section of Pekin duck and Liancheng white duck. (B–F) The most representative spatial distribution differences of lipid molecules. (G–I) Mass spectra corresponding to lipid molecules with different spatial distribution.

medicinal and health functions of Liancheng white duck from a certain perspective, but the molecular mechanisms by which they affect meat quality and toughness still need further investigation.

IMF deposition is closely related to lipid composition. Studies have shown that changes in IMF content led to changes the lipid profiles of meat (Li et al., 2020a, 2021a). Present study found that the IMF content in breast muscle of Pekin duck was significantly higher than that of Liancheng white duck ($P < 0.01$). The results of lipidomic analysis showed that GPs and GLs may be the reasons for differences in IMF deposition between varieties. The study reported that compared to Duroc pigs the GPs were upregulated in Luchuan pigs

which containing higher IMF and GL, and the difference in GPs may be related to glycerophosphate metabolism (Zhang et al., 2021).

It was reported that the contents of TG, PC, PE, and SM were changed during the processing of dry-cured mutton ham, in which the metabolism of glycerophospholipid and sphingolipid played a critical role (Guo et al., 2022). Therefore, the variations in lipids between Peking duck and Liancheng white duck may be a reason for the difference in meat flavor and nutrition. Furthermore, among the lipids with significant differences, TG had the most number, and all of them were significantly upregulated in Pekin duck breast muscle, TG is a neutral lipid that accumulates in lipid droplets to store fat

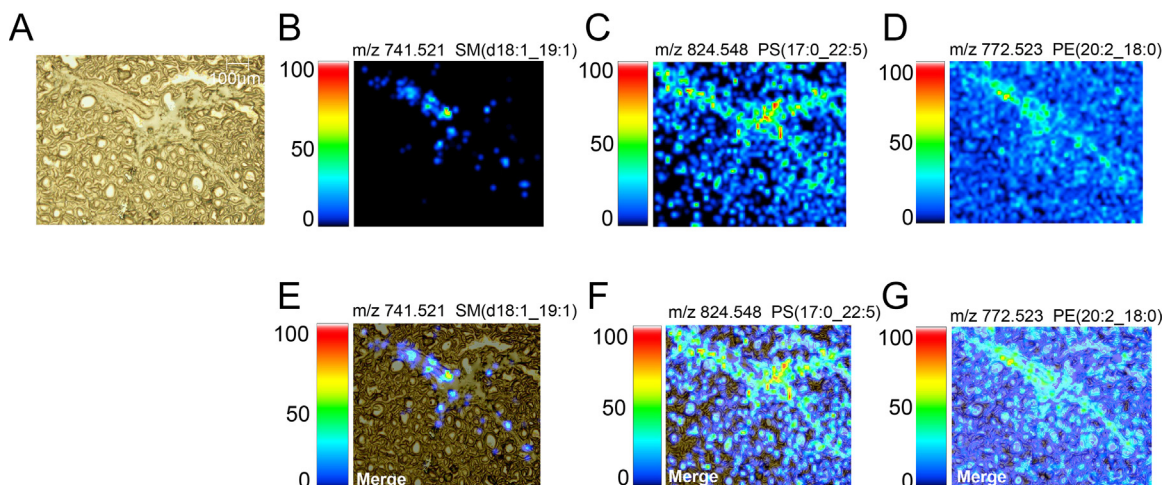


Figure 8. MS images of representative lipid metabolites in breast muscle of duck.

(Kuerschner et al., 2008; Tsai et al., 2017), the above results demonstrate the high lipid deposition capacity of Pekin duck. Long-chain polyunsaturated fatty acids (LCPUFA), such as docosahexaenoic acid (C22:6, DHA), which more abundant in Liancheng white duck. Studies have shown that LCPUFA has a positive effect on physiological function such as in neurodevelopment, immune system, as well as in hypertension, arthritis, depression, myocardial infarction, thrombosis, and other diseases (Janssen and Kiliaan, 2014; Miles et al., 2021), this to some extent explains the high medicinal function of Liancheng white duck.

The distribution of lipids in meat was probed by spatial metabolomics (spatial resolution: $50\ \mu\text{m} \times 50\ \mu\text{m}$) and they were found to be uniformly distributed in the meat. Interestingly, after further improving spatial resolution ($10\ \mu\text{m} \times 10\ \mu\text{m}$), it was found that some lipid molecules are specifically distributed on the connective tissue membrane. Such SM (d18:1_19:1), as a sphingolipid, it is mainly enriched in the connective tissue membrane. Sphingolipid is not only an important constituent of membranes, but a dietary component, its metabolites include ceramide (Cer), sphingosine (Sph), and sphingosine-phosphate (S1P) (Fayyaz et al., 2014), which are involved in the regulation of a variety of physiologic functions, such immune and inflammatory reactions (Hernández-Corbacho et al., 2017; Tan-Chen et al., 2020). Recent studies have found that sphingolipid and its metabolites play an essential role in muscle development (Nagata et al., 2006; Ishida et al., 2016). Therefore, the breast muscle of Liancheng white duck with thicker perimysium contains higher sphingolipid, which explained from physical structure, lipomics, and spatial metabolomics that Liancheng white duck has medicinal and health functions.

In summary, we first investigated the development pattern of duck breast muscle and analyzed the meat quality of Pekin duck and Liancheng white duck, and found significant differences in IMF content and WBSF. Based on this, we analyzed the ultrastructure of skeletal muscle by SEM and TEM and further explained that collagen architecture had a certain effect on meat toughness. In addition, a total 333 significantly different lipid molecules might be affected by IMF through targeted lipidomics analysis. Among the lipids with significant differences, TGs had the most number and were significantly upregulated in Pekin duck, it is a neutral lipid that accumulates in lipid droplets to store fat, which demonstrates the high lipid deposition capacity of Pekin duck. LCPUFAs were more abundant in Liancheng white duck, which to some extent explains the high medicinal function of Liancheng white duck. Spatial metabolomics found that most lipid molecules were uniformly distributed in meat, but some were specifically distributed in connective tissue. Our findings could contribute to a better understanding the relationship between skeletal muscle architecture and meat toughness, increased the knowledge of the lipidomic characteristics and provide a basis for duck meat authentication. However, meat quality research is complex. The taste,

texture, juiciness, appearance, and odor are all important factors affecting the quality of meat. Our research is still superficial, and further in-depth and more systematic research should be carried out.

ACKNOWLEDGMENTS

This work was supported by grants from the National Natural Science Foundation of China (31972523), the Young Top-notch Talent Project of the National Ten Thousand Talent Program, the China Agriculture Research System of MOF and MARA (CARS-42), and the CAAS Innovation Team Project (ASTIP-IAS-9, CAAS-ZDRW202104).

DISCLOSURES

The authors declare that they have no competing interests.

SUPPLEMENTARY MATERIALS

Supplementary material associated with this article can be found in the online version at [doi:10.1016/j.psj.2023.103106](https://doi.org/10.1016/j.psj.2023.103106).

REFERENCES

- Albrecht, E., F. Teuscher, K. Ender, and J. Wegner. 2006. Growth- and breed-related changes of muscle bundle structure in cattle. *J. Anim. Sci.* 84:2959–2964.
- Albu, M. D. L. G., Z. Vuluga, D. M. Panaitescu, D. M. Vuluga, A. Cășărică, and M. Ghiurea. 2014. Morphology and thermal stability of bacterial cellulose/collagen composites. *Cent. Eur. J. Chem.* 12:968–975.
- Blackburn, D. M., F. Lazure, A. H. Corchado, T. J. Perkins, H. S. Najafabadi, and V. D. Soleimani. 2019. High-resolution genome-wide expression analysis of single myofibers using SMART-Seq. *J. Biol. Chem.* 294:20097–20108.
- Breslin, P. A. 2013. An evolutionary perspective on food and human taste. *Curr. Biol.* 23:R409–R418.
- Fan, L., M. Peng, X. Zhou, H. Wu, and S. Liu. 2014. Modification of carboxymethyl cellulose Grafted with collagen peptide and its antioxidant activity. *Carbohydr. Polym.* 112:32–38.
- Fayyaz, S., L. Japtok, and B. Kleuser. 2014. Divergent role of sphingosine 1-phosphate on insulin resistance. *Cell Physiol. Biochem.* 34:134–147.
- Guo, X., D. Shi, C. Liu, Y. Huang, Q. Wang, J. Wang, L. Pei, and S. Lu. 2022. UPLC-MS-MS-based lipidomics for the evaluation of changes in lipids during dry-cured mutton ham processing. *Food Chem.* 377:131977.
- Hernández-Corbacho, M. J., M. F. Salama, D. Canals, C. E. Senkal, and L. M. Obeid. 2017. Sphingolipids in mitochondria. *Biochim. Biophys. Acta Mol. Cell. Biol. Lipids* 1862:56–68.
- Hitosugi, S., K. Tsuda, H. Okabayashi, and Y. Tanabe. 2007. Phylogenetic relationships of mitochondrial DNA cytochrome b gene in East Asian ducks. *J. Poultry Sci.* 44:141–145.
- Huo, W., K. Weng, T. Gu, Y. Zhang, Y. Zhang, G. Chen, and Q. Xu. 2021. Effect of muscle fiber characteristics on meat quality in fast- and slow-growing ducks. *Poult. Sci.* 100:101264.
- Ishida, Y., Y. Kiyokawa, T. Asai, and N. Oku. 2016. Ameliorating effects of sphingomyelin-based liposomes on sarcopenia in senescence-accelerated mice. *Biol. Pharm. Bull.* 39:786–793.
- Janssen, C. I., and A. J. Kiliaan. 2014. Long-chain polyunsaturated fatty acids (LCPUFA) from genesis to senescence: the influence of LCPUFA on neural development, aging, and neurodegeneration. *Prog. Lipid Res.* 53:1–17.

- Jia, W., Z. Fan, Q. Shi, R. Zhang, X. Wang, and L. Shi. 2021. LC-MS-based metabolomics reveals metabolite dynamic changes during irradiation of goat meat. *Food Res. Int.* 150:110721.
- Kragstrup, T. W., M. Kjaer, and A. L. Mackey. 2011. Structural, biochemical, cellular, and functional changes in skeletal muscle extracellular matrix with aging. *Scand. J. Med. Sci. Sports* 21:749–757.
- Kuerschner, L., C. Moessinger, and C. Thiele. 2008. Imaging of lipid biosynthesis: how a neutral lipid enters lipid droplets. *Traffic* 9:338–352.
- Li, B., E. K. Neumann, J. Ge, W. Gao, H. Yang, P. Li, and J. V. Sweedler. 2018. Interrogation of spatial metabolome of *Ginkgo biloba* with high-resolution matrix-assisted laser desorption/ionization and laser desorption/ionization mass spectrometry imaging. *Plant Cell Environ.* 41:2693–2703.
- Li, R., Z. Sun, Y. Zhao, L. Li, X. Yang, J. Cen, S. Chen, C. Li, and Y. Wang. 2021b. Application of UHPLC-Q-TOF-MS/MS metabolomics approach to investigate the taste and nutrition changes in tilapia filets treated with different thermal processing methods. *Food Chem.* 356:129737.
- Li, J., C. Tang, Q. Zhao, Y. Yang, F. Li, Y. Qin, X. Liu, X. Yue, and J. Zhang. 2020a. Integrated lipidomics and targeted metabolomics analyses reveal changes in flavor precursors in psoas major muscle of castrated lambs. *Food Chem.* 333:127451.
- Li, J., J. Zhang, Y. Yang, J. Zhu, W. He, Q. Zhao, C. Tang, Y. Qin, and J. Zhang. 2021a. Comparative characterization of lipids and volatile compounds of Beijing Heilium and Laiwu Chinese black pork as markers. *Food Res. Int.* 146:110433.
- Li, S., N. Zhu, C. Tang, H. Duan, Y. Wang, G. Zhao, J. Liu, and Y. Ye. 2020b. Differential distribution of characteristic constituents in root, stem and leaf tissues of *Salvia miltiorrhiza* using MALDI mass spectrometry imaging. *Fitoterapia* 146:104679.
- Maltin, C., D. Balcerzak, R. Tilley, and M. Delday. 2003. Determinants of meat quality: tenderness. *Proc. Nutr. Soc.* 62:337–347.
- Matarneh, S. K., S. L. Silva, and D. E. Gerrard. 2021. New insights in muscle biology that alter meat quality. *Annu. Rev. Anim. Biosci.* 9:355–377.
- Miles, E. A., C. E. Childs, and P. C. Calder. 2021. Long-chain polyunsaturated fatty acids (LCPUFAs) and the developing immune system: a narrative review. *Nutrients* 13:247.
- Moloney, A. P., M. T. Mooney, J. P. Kerry, and D. J. Troy. 2001. Producing tender and flavoursome beef with enhanced nutritional characteristics. *Proc. Nutr. Soc.* 60:221–229.
- Muroya, S., S. Ueda, T. Komatsu, T. Miyakawa, and P. Ertbjerg. 2020. MEATabolomics: muscle and meat metabolomics in domestic animals. *Metabolites* 10:188.
- Nagata, Y., T. A. Partridge, R. Matsuda, and P. S. Zammit. 2006. Entry of muscle satellite cells into the cell cycle requires sphingolipid signaling. *J. Cell Biol.* 174:245–253.
- Nishimura, T. 2015. Role of extracellular matrix in development of skeletal muscle and postmortem aging of meat. *Meat Sci.* 109:48–55.
- Norris, J. L., and R. M. Caprioli. 2013. Analysis of tissue specimens by matrix-assisted laser desorption/ionization imaging mass spectrometry in biological and clinical research. *Chem. Rev.* 113:2309–2342.
- Ohtani, O., T. Ushiki, T. Taguchi, and A. Kikuta. 1988. Collagen fibrillar networks as skeletal frameworks: a demonstration by cell-maceration/scanning electron microscope method. *Arch. Histol. Cytol.* 51:249–261.
- Orzechowska, B., D. Wojtysiak, W. Migdał, and M. Tyra. 2008. Relationships between muscle fibre characteristics and physico-chemical properties of longissimus lumborum muscle and growth rate in pig fatteners of three breeds. *Anim. Sci. Pap. Rep.* 26:277–285.
- Ouyang, Q., Q. Chen, S. Ke, L. Ding, X. Yang, P. Rong, W. Feng, Y. Cao, Q. Wang, M. Li, S. Su, W. Wei, M. Liu, J. Liu, X. Zhang, J. Z. Li, H. Y. Wang, and S. Chen. 2023. Rab8a as a mitochondrial receptor for lipid droplets in skeletal muscle. *Dev. Cell* 58:289–305 e286.
- Payne, G. W., and S. E. Bearden. 2006. The microcirculation of skeletal muscle in aging. *Microcirculation* 13:275–277.
- Pereira, P. M., and A. F. Vicente. 2013. Meat nutritional composition and nutritive role in the human diet. *Meat Sci.* 93:586–592.
- Purslow, P. P. 2014. New developments on the role of intramuscular connective tissue in meat toughness. *Annu. Rev. Food Sci. Technol.* 5:133–153.
- Ramanathan, R., S. P. Suman, and C. Faustman. 2020. Biomolecular interactions governing fresh meat color in post-mortem skeletal muscle: a review. *J. Agric. Food Chem.* 68:12779–12787.
- Rambold, A. S., S. Cohen, and J. Lippincott-Schwartz. 2015. Fatty acid trafficking in starved cells: regulation by lipid droplet lipolysis, autophagy, and mitochondrial fusion dynamics. *Dev. Cell* 32:678–692.
- Roy, B. C., B. Walker, M. M. Rahman, H. L. Bruce, and L. McMullen. 2018. Role of myofibers, perimysium and adipocytes in horse meat toughness. *Meat Sci.* 146:109–121.
- Sasaki, K., M. Motoyama, and T. Narita. 2012. Increased intramuscular fat improves both 'chewiness' and 'hardness' as defined in ISO5492:1992 of beef Longissimus muscle of Holstein × Japanese black F1 steers. *Anim. Sci. J.* 83:338–343.
- Schiaffino, S., K. A. Dyar, S. Ciciliot, B. Blaauw, and M. Sandri. 2013. Mechanisms regulating skeletal muscle growth and atrophy. *FEBS J.* 280:4294–4314.
- Tan-Chen, S., J. Guitton, O. Bourron, H. Le Stunff, and E. Hajdouch. 2020. Sphingolipid metabolism and signaling in skeletal muscle: from physiology to physiopathology. *Front. Endocrinol. (Lausanne)* 11:491.
- Tang, H., D. Liu, H. Zhang, W. Fan, J. Hu, Y. Xu, Z. Guo, W. Huang, S. Hou, and Z. Zhou. 2023. Genome-wide association studies demonstrate the genes associated with perimysial thickness in ducks. *Anim. Genet.* 54:363–374.
- Tsai, T. H., E. Chen, L. Li, P. Saha, H. J. Lee, L. S. Huang, G. S. Shelness, L. Chan, and B. H. Chang. 2017. The constitutive lipid droplet protein PLIN2 regulates autophagy in liver. *Autophagy* 13:1130–1144.
- Wang, B., Y. Wang, S. Zuo, S. Peng, Z. Wang, Y. Zhang, and H. Luo. 2021. Untargeted and targeted metabolomics profiling of muscle reveals enhanced meat quality in artificial pasture grazing tan lambs via rescheduling the rumen bacterial community. *J. Agric. Food Chem.* 69:846–858.
- Wheeler, T. L., S. D. Shackelford, and M. Koohmaraie. 2000. Variation in proteolysis, sarcomere length, collagen content, and tenderness among major pork muscles. *J. Anim. Sci.* 78:958–965.
- Wojtysiak, D. 2013. Effect of age on structural properties of intramuscular connective tissue, muscle fibre, collagen content and meat tenderness in pig longissimus lumborum muscle. *Folia Biol. (Kra-kow)* 61:221–226.
- Yuan, Y. L., J. L. Li, W. H. Zhang, C. Li, F. Gao, and G. H. Zhou. 2012. A comparison of slaughter performance and meat quality of pigs immunised with a gonadotrophin-releasing factor vaccine against boar taint with physically castrated pigs. *Anim. Prod. Sci.* 52:911–916.
- Zhang, Z., Q. Liao, Y. Sun, T. Pan, S. Liu, W. Miao, Y. Li, L. Zhou, and G. Xu. 2021. Lipidomic and transcriptomic analysis of the longissimus muscle of Luchuan and Duroc pigs. *Front. Nutr.* 8:667622.
- Zhou, Z., M. Li, H. Cheng, W. Fan, Z. Yuan, Q. Gao, Y. Xu, Z. Guo, Y. Zhang, J. Hu, H. Liu, D. Liu, W. Chen, Z. Zheng, Y. Jiang, Z. Wen, Y. Liu, H. Chen, M. Xie, Q. Zhang, W. Huang, W. Wang, S. Hou, and Y. Jiang. 2018. An intercross population study reveals genes associated with body size and plumage color in ducks. *Nat. Commun.* 9:2648.